Title

In vitro 0N4R tau fibrils contain a monomorphic β-sheet core enclosed by dynamically heterogeneous fuzzy coat segments

Journal

Proceedings of the National Academy of Sciences of the United States of America, 116(33)

ISSN

0027-8424

Authors

Dregni, Aurelio J
Mandala, Venkata S
Wu, Haifan
et al.

Publication Date

2019-08-13

DOI

10.1073/pnas.1906839116

Peer reviewed

In vitro 0N4R tau fibrils contain a monomorphic β-sheet core enclosed by dynamically heterogeneous fuzzy coat segments

Aurelio J. Dregni[a,1], Venkata S. Mandala[a,1], Haifan Wu[b,1], Matthew R. Elkins[a], Harrison K. Wang[a], Ivan Hung[c], William F. DeGrado[b,2], and Mei Hong[a,2]

[a]Department of Chemistry, Massachusetts Institute of Technology, Cambridge, MA 02139; [b]Department of Pharmaceutical Chemistry, University of California, San Francisco, CA 94158; and [c]National High Magnetic Field Laboratory, Tallahassee, FL 32310

Contributed by William F. DeGrado, June 5, 2019 (sent for review April 24, 2019; reviewed by Robert Tycko and Markus Zweckstetter)

Misfolding of the microtubule-binding protein tau into filamentous aggregates is characteristic of many neurodegenerative diseases such as Alzheimer's disease and progressive supranuclear palsy. Determining the structures and dynamics of these tau fibrils is important for designing inhibitors against tau aggregation. Tau fibrils obtained from patient brains have been found by cryo-electron microscopy to adopt disease-specific molecular conformations. However, in vitro heparin-fibrillized 2N4R tau, which contains all four microtubule-binding repeats (4R), was recently found to adopt polymorphic structures. Here we use solid-state NMR spectroscopy to investigate the global fold and dynamics of heparin-fibrillized 0N4R tau. A single set of ^{13}C and ^{15}N chemical shifts was observed for residues in the four repeats, indicating a single β-sheet conformation for the fibril core. This rigid core spans the R2 and R3 repeats and adopts a hairpin-like fold that has similarities to but also clear differences from any of the polymorphic 2N4R folds. Obtaining a homogeneous fibril sample required careful purification of the protein and removal of any proteolytic fragments. A variety of experiments and polarization transfer from water and mobile side chains indicate that 0N4R tau fibrils exhibit heterogeneous dynamics: Outside the rigid R2–R3 core, the R1 and R4 repeats are semirigid even though they exhibit β-strand character and the proline-rich domains undergo large-amplitude anisotropic motions, whereas the two termini are nearly isotropically flexible. These results have significant implications for the structure and dynamics of 4R tau fibrils in vivo.

solid-state NMR | conformational polymorphism | polymorphism

Tau is a microtubule-binding protein that aggregates into intraneuronal filaments in a number of neurodegenerative diseases called tauopathies. The protein contains four microtubule-binding repeats, R1 to R4 (1), a subset of which aggregate into cross-β fibrils. The rest of the protein is largely disordered, as shown by the appearance of a "fuzzy coat" in electron micrographs (2). Tau has six isoforms in the adult human brain, which are characterized by the inclusion of 0 to 2 acidic 29-residue inserts in the N-terminal half of the protein (0N, 1N, or 2N tau), and inclusion (4R tau) or exclusion (3R tau) of the R2 repeat domain (3). The longest isoform, 2N4R tau, contains 441 residues, whose numbering is used for all isoforms (Fig. 1*A*). Tauopathies are distinguished by the isoforms involved. For example, Pick's disease (PiD) fibrils contain primarily 3R isoforms, progressive supranuclear palsy (PSP) fibrils contain 4R isoforms, whereas Alzheimer's disease (AD) and chronic traumatic encephalopathy (CTE) fibrils contain a mixture of 3R and 4R isoforms (4).

Tau fibrils in diseased brains propagate their misfolded conformations by recruiting monomeric tau to adopt the same misfolded structures (5–7). To understand the molecular mechanism of this propagation, it is crucial to determine the 3D structures of tau aggregates and establish whether each tauopathy has a unique structure, and whether different tauopathies share conserved structural elements. Given the multiple isoforms of tau and the polymorphic structures of other amyloid-forming proteins such as Aβ in response to the environment (8, 9), one might expect tau fibril structures to be variable both between different diseases and within each disease. However, recent cryo-electron microscopy (cryo-EM) data showed that the AD tau structure (10) differs from the PiD tau structure (11), but multiple AD brains appear to adopt the same fibril core structure (12). This observation suggests that tau fibril structures may be conserved within a disease, despite the mixed isoform nature of AD and other 3R/4R tauopathies.

Recombinant tau monomers can form fibrils in the presence of anionic cofactors such as heparin, a sulfated glycosaminoglycan polymer (13). Heparin-fibrillized tau is morphologically similar to AD patient-derived fibrils, and thus it could in principle serve as a model system for elucidating the folding pathway and structures of tau fibrils. However, a recent cryo-EM study reported that heparin-fibrillized 2N4R tau exhibits at least 4 molecular structures (14): The dominant polymorph represents less than 45% of all fibrils and none of the structures are similar to the in vivo tau structures of AD or CTE (10, 15). It is paradoxical

Significance

The microtubule-binding protein tau misfolds into filamentous aggregates in many neurodegenerative diseases. Understanding the structure and dynamics of tau fibrils is important for designing anti-tau inhibitors. Patient-brain-derived tau fibrils have been shown to adopt disease-specific molecular conformations, but in vitro heparin-fibrillized tau was recently proposed to exhibit significant structural polymorphism. Using solid-state NMR, we show that the β-sheet core of heparin-fibrillized 0N4R tau adopts a single molecular conformation that encompasses the second and third microtubule-binding repeats, and both cysteine residues in the protein are involved in side-chain packing with other β-sheet residues. Extensive characterization of the protein dynamics indicates that these tau fibrils are heterogeneously dynamic, and the first and fourth microtubule-binding repeats are semirigid while retaining β-sheet character.

Author contributions: W.F.D. and M.H. designed research; A.J.D., V.S.M., H.W., M.R.E., and I.H. performed research; A.J.D., V.S.M., H.W., H.K.W., and M.H. analyzed data; and A.J.D., V.S.M., H.W., W.F.D., and M.H. wrote the paper.

Reviewers: R.T., NIH; and M.Z., Max Planck Institute for Biophysical Chemistry.

Conflict of interest statement: I.H., in his role as a staff scientist at the National High Magnetic Field Laboratory to assist external users, has a previous copublication with Robert Tycko.

[1]A.J.D., V.S.M., and H.W. contributed equally to this work.

[2]To whom correspondence may be addressed. Email: william.degrado@ucsf.edu or meihong@mit.edu.

This article contains supporting information online at www.pnas.org/lookup/suppl/doi:10.1073/pnas.1906839116/-/DCSupplemental.

Published online July 29, 2019.

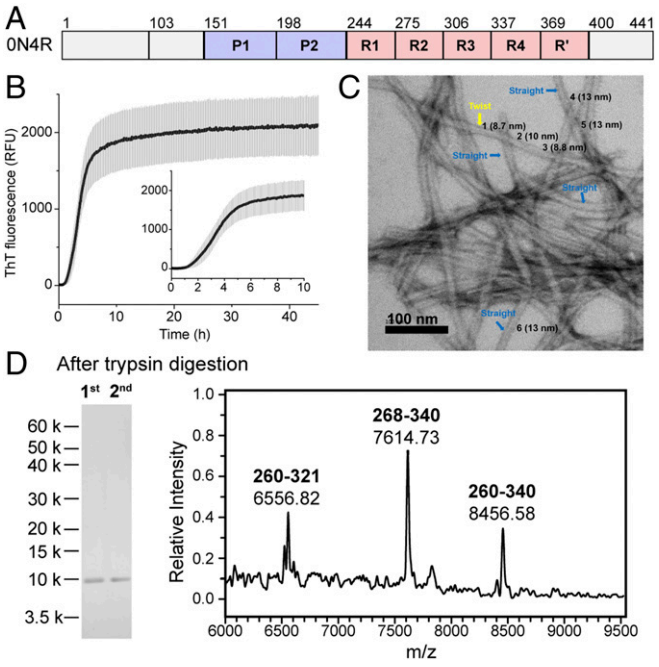

Fig. 1. Heparin-fibrillized 0N4R tau forms well-ordered amyloid fibrils with a single dominant ultrastructural morphology. (*A*) Amino acid sequence diagram of 0N4R tau. Residue 44 is followed by 103, based on the 2N4R numbering scheme. (*B*) ThT fluorescence shows a lag time of about 1 h during fibril formation. (*C*) Representative negative-stain electron micrograph of 0N4R tau fibrils, showing predominantly straight fibrils with a diameter of ∼13 nm. (Scale bar: 100 nm.) (*D*) Trypsin digestion of multiple batches of tau fibrils reproducibly show a band at ∼10 kDa in the SDS/PAGE gel. The mass spectrum indicates that a segment corresponding to residues 268 to 340 is the main species protected from trypsin.

that a mixture of tau isoforms formed in the complex environment of the brain is monomorphic whereas a single tau isoform fibrillized under controlled conditions is polymorphic. For comparison, AD brain-derived Aβ40 fibrils show a predominant structure within each brain but can differ between different brains (16), between different clinical subtypes (17, 18), and between vascular and parenchymal compartments of a given brain (19). This in vivo polymorphism is qualitatively consistent with the polymorphism of in vitro Aβ40 fibrils (20–22). Therefore, the relationship between in vitro and in vivo tau fibril structure distribution is unclear. Moreover, little is known about the dynamics of the non-microtubule-binding regions of tau. Trypsin digestion data of fibrils from various tauopathies indicate that the trypsin-resistant core contains 90 to 150 residues (23) out of 352 to 441 residues for the full-length protein, and thus the majority of the protein in the fibril is dynamic and disordered. Atomic force microscopy data suggested a model of a 2-layered polyelectrolyte brush for this disordered fuzzy coat, where the rigid core is surrounded by a stiff, dense, and basic region formed by the proline (Pro)-rich domains (residues 151 to 243), which is in turn surrounded by a softer and less dense acidic layer formed by the N-terminal region (24). Solution NMR studies of tau protofibrils found residues 1 to 160 and 400 to 441 to be highly dynamic, but most other residues were not detected (25–27). To date, the dynamic differences between various domains of tau fibrils are poorly understood, and the structure of the microtubule-binding repeats that are unresolved in the cryo-EM maps remains unknown.

Here we present a site-specific study of the molecular conformation and dynamics of a full-length 4R tau fibril formed using heparin. The 2D and 3D correlation solid-state NMR (SSNMR) spectra and chemical shift analysis indicate that in vitro heparin-fibrillized 0N4R tau adopts a single β-sheet conformation for the fibril core, in contrast to the previous polymorphic results. This monomorphic fold shares a common β-sheet steric zipper with the 2N4R structures but differs in the region that contains 1 of 2 cysteines in the protein, C291. Biochemical data indicate that high chemical homogeneity was required to obtain conformationally homogeneous fibrils, and trace proteolytic contaminates can lead to pronounced heterogeneity in fibril morphology. We show that 0N4R tau fibrils contain 4 dynamically distinct domains: the R2 and R3 repeats form the rigid core, the R1 and R4 repeats are semirigid but β-sheet in character, and the proline-rich domains are anisotropically mobile, whereas the N and C termini are nearly isotropically flexible. These results have implications for the possible structure of the in vivo 4R tau, the sequence determinant of the structure distribution of the tau fibril core, and the mechanism with which the dynamic domains might impact the 3D fold of the β-sheet core.

Results

0N4R Tau Forms a Single Ultrastructural Fibril Morphology In Vitro. We expressed recombinant 0N4R tau with high purity using a combination of heat denaturation (28), cation exchange chromatography, and reversed-phase high-performance liquid chromatography (HPLC). Fibrils were formed by incubating tau at a low concentration of 0.4 mg/mL with 0.125 mg/mL heparin under reducing conditions to prevent Cys oxidation. The solution was incubated at 37 °C with agitation for 3 d. Thioflavin-T (ThT) fluorescence data showed that fibril formation had a lag time of about 1 h and was mostly completed in about 8 h (Fig. 1*B*). Negative-stain transmission electron microscopy (TEM) images show straight, unbranched fibrils with a diameter of 13 nm as the dominant species (Fig. 1*C*). Trypsin digestion followed by sodium dodecyl sulfate polyacrylamide gel electrophoresis (SDS/PAGE) analysis reproducibly yielded a single band (<10 kDa) (Fig. 1*D*), whose mass spectrum indicates that the main trypsin-resistant species is a segment corresponding to residues 268 to 340.

0N4R Tau Contains a Monomorphic β-Sheet Core Coexisting with a Dynamically Disordered Domain. We labeled 0N4R tau with ^{13}C, ^{15}N, except for Gly, Glu, and Lys residues to simplify NMR resonance assignment. Experiments that employ ^{1}H-^{13}C cross-polarization (CP) and dipolar polarization transfer selectively detect immobilized residues, whereas pulse sequences such as total correlation spectroscopy (TOCSY) and insensitive nuclei enhanced by polarization transfer (INEPT) use scalar coupling for polarization transfer and selectively detect highly dynamic residues. Fig. 2*A* shows the 2D ^{13}C-^{13}C spin-diffusion correlation spectrum. Two strong Cys Cα-Cβ peaks are resolved whose Cβ chemical shifts correspond to reduced thiols. Since there are only two cysteines in tau, C291 in R2 and C322 in R3, the presence of two Cys Cα-Cβ cross-peaks strongly suggests that 0N4R tau has a single fibril core conformation that encompasses R2 and R3. In the Ser Cα-Cβ chemical shift range, at least 10 correlation peaks are resolved, in good agreement with the presence of 12 Ser residues within the R1–R4 repeats. Consistent with the 2D ^{13}C-^{13}C correlation spectrum, a 2D ^{15}N-$^{13}C\alpha$ dipolar correlation spectrum shows more than 50 cross-peaks (see Fig. 5*G*), suggesting that the β-sheet core of 0N4R tau contains at least 50 residues. The isolated peaks in these spectra show ^{13}C and ^{15}N line widths of 0.5 to 0.7 ppm and 1.1 to 1.5 ppm, respectively, indicating that the rigid core of the protein is structurally homogeneous.

To detect highly dynamic residues, we measured a 2D ^{13}C-^{13}C TOCSY spectrum, using scalar coupling for polarization transfer (Fig. 2*B*). The spectrum shows well-resolved signals at random coil ^{13}C chemical shifts and can be readily assigned based on the connectivity patterns and the characteristic chemical shifts of

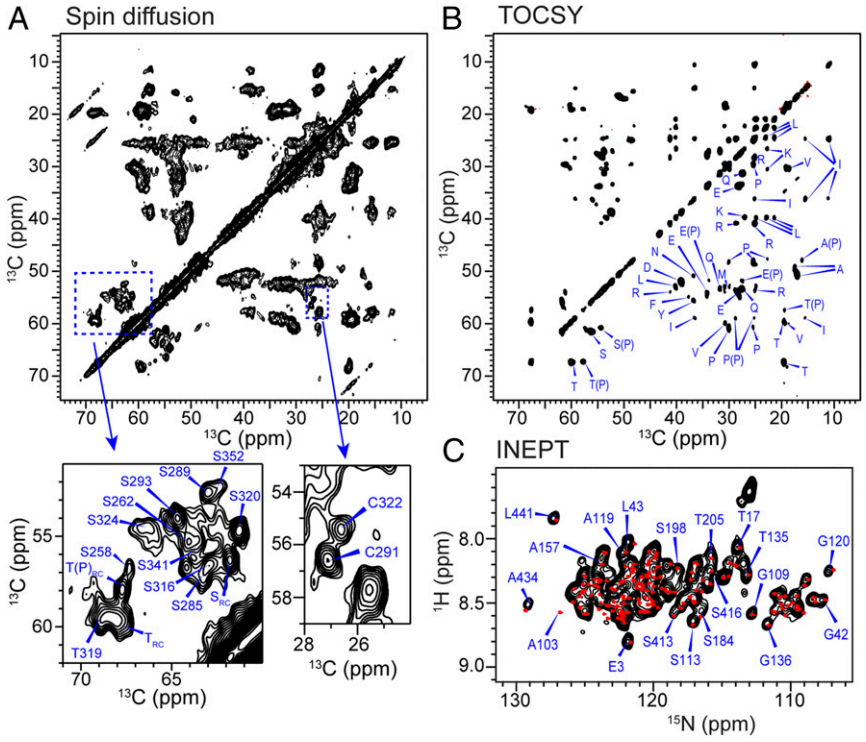

Fig. 2. Two-dimensional SSNMR spectra of 0N4R tau fibrils indicate the coexistence of a rigid β-sheet core with dynamic random coil domains. (*A*) Two-dimensional ^{13}C-^{13}C correlation spectrum with 23-ms ^{13}C spin diffusion. (*Inset*) Expanded Ser/Thr and Cys regions where assignments obtained from 3D spectra are indicated. A single set of chemical shifts is observed. (*B*) Two-dimensional ^{13}C-^{13}C TOCSY spectrum shows narrow peaks at random coil chemical shifts, indicating the presence of dynamically disordered residues. Amino acid type assignments are indicated for the most characteristic chemical shifts. (*C*) Two-dimensional ^{1}H-^{15}N INEPT spectrum. Previously reported solution NMR chemical shifts of the dynamic residues (red) in 2N4R tau protofibrils (25) are overlaid to indicate the excellent agreement with the 0N4R tau chemical shifts. Assignments of resolved peaks are shown.

amino acids. A single set of chemical shifts is observed for most amino acid types, indicating that the same residue types have similar dynamically averaged conformations. A small number of residue types show two sets of signals, one occurring at averaged random-coil chemical shifts and the other at chemical shifts known for residues that are followed by a Pro (29, 30). We also measured a 2D ^{1}H-^{15}N INEPT correlation spectrum (Fig. 2*C*) to detect the highly dynamic segments in the protein. Importantly, the observed ^{1}H and ^{15}N chemical shifts have excellent agreement with previously reported solution NMR chemical shifts of 2N4R protofilaments (25, 26), despite the fact that N1 and N2 domains are absent in the current construct. The only chemical shift difference between the two proteins is observed at A103, which is preceded by T102 in 2N4R tau but by K44 in 0N4R tau. The almost complete identity of these chemical shifts suggests that the fuzzy coats of 0N4R and 2N4R tau fibrils have similar disordered structures.

The Fibril Core of 0N4R Tau Spans R2 and R3 and Has a Unique 3D Fold. To obtain unambiguous evidence that the β-sheet core of 0N4R tau is monomorphic, we measured 3 sets of 3D ^{15}N-^{13}C correlation spectra. The intraresidue NCACX experiment combines with the interresidue NCOCX and CONCA correlation experiments to allow sequence-specific assignment of ^{15}N and ^{13}C chemical shifts (31–34). Representative strips from the 3D spectra are shown in Fig. 3*A* and *SI Appendix*, Fig. S1. The experiments were conducted using ^{15}N-^{13}C dipolar polarization transfer, which selectively detects only the most rigid residues (31). The two cysteines in the protein, C291 and C322, are unambiguously assigned (*SI Appendix*, Fig. S2 *A* and *B*): Each Cys has a single set of resonances whose Cβ chemical shifts (26.9 ppm for C291 and 26.5 ppm for C322) correspond to reduced thiols. R349 and Y310 have well-resolved Cζ signals at 157 ppm, which show a single set of cross-peaks with the respective carbons in each residue (*SI Appendix*, Fig. S2*C*). The hexapeptide motifs of R2 (V275–N279) and R3 (V306–Y310) manifest strong signals, indicating that these segments are immobilized (35). In total, we assigned 66 residues between S258 and T361 (Fig. 3*B* and *SI Appendix*, Table S1), and all strong signals were assigned to a single conformation. Out of the 38 unassigned residues in this region, 19 are not labeled, 12 are next to an unlabeled residue and thus are not detected in the NCOCX and CONCA spectra, and 4 are prolines, which lack an amide proton and thus show weak intensities in these ^{15}N-^{13}C correlation spectra. Based on the signal-to-noise ratios of the assigned strong peaks such as C291 and S293 versus unassigned peaks such as 2 Ser peaks in the 2D NCA spectrum (see Fig. 5*G*), we estimate that the major conformation represents at least 80% of the fibrils. Many unassigned peaks likely result from R1, R4, and R′ residues (discussed below) instead of a second conformation, and therefore we expect the true population of the main conformer to exceed 90%.

The assigned Cα chemical shifts (Fig. 3*B*) are smaller than the random coil chemical shifts while the Cβ chemical shifts are larger, indicating that all assigned residues adopt β-sheet conformation. The chemical-shift–derived (φ, ψ) torsion angles (36) indicate six β-strands (β1–β6) (Fig. 3*C* and *SI Appendix*, Table S2): β1 covers the R2 hexapeptide motif ^{275}VQIINK^{280}, which is important for amyloid formation (35), and β6 spans the ^{336}QVEVK^{340} segment at the beginning of R4. These β-strand positions differ from those of the in vitro 2N4R tau fibrils (discussed below) as well as the AD tau fibrils for the common R3 and R4 domains (10). The ^{13}C and ^{15}N chemical shifts of full-length 0N4R tau also differ significantly from the chemical shifts

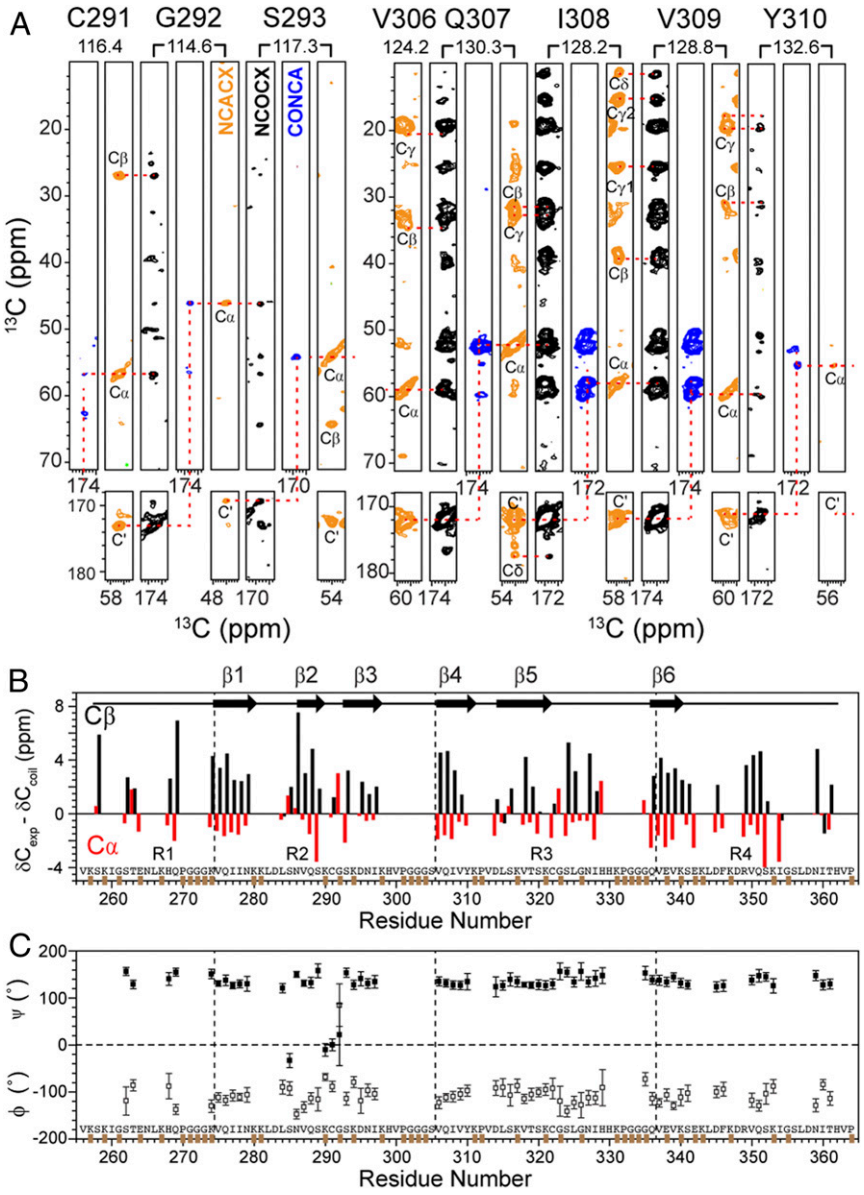

Fig. 3. 0N4R tau fibrils exhibit a single β-sheet core conformation. (*A*) Representative strips from the 3D NCACX (orange), NCOCX (black), and CONCA (blue) spectra for R2 and R3 residues. (*B*) Secondary-structure-dependent Cα and Cβ chemical shifts of assigned residues indicate the presence of 6 β-strands (arrows) in the 4 repeat domains. (*C*) Chemical-shift-derived backbone torsion angles (36). Error bars indicate the precision of the TALOS-N prediction. The positions of unlabeled or weakly labeled G, E, and K residues and P residues are marked in brown on the *x* axis.

of two truncated tau constructs, K19 and an R3-only peptide (*SI Appendix*, Fig. S3) (37–39). Therefore, the fibril core of 0N4R tau is distinct from the folds of both in vivo tau fibrils and in vitro truncated tau fibrils studied so far.

To determine the overall 3D shape of the 0N4R fibril core, we measured 2D ^{13}C-^{13}C and 3D NCACX correlation spectra using a long ^{13}C spin diffusion mixing time of 500 ms. We also measured a 3D ^{13}C-^{13}C-^{13}C (CCC) correlation spectrum with ^{13}C spin diffusion mixing times of 100 ms and 500 ms. The 2D CC spectrum shows cross-peaks between G292 Cα and V309 Cγ (Fig. 4*A*) and between S293 Cβ and Q307 Cδ, indicating close proximities between the β3 strand in R2 and the β4 strand, which corresponds to the R3 hexapeptide motif. The 3D NCACX spectrum shows many sequential and medium-range cross-peaks but in addition shows long-range cross-peaks between S320 Cα and V275 Cβ or Q276 Cγ and between V318 Cα and I277 or I278 Cγ2 (Fig. 4*B*). The 3D CCC spectrum (Fig. 4*C*) resolved many additional long-range correlation peaks such as Q276-S320, C322-V275, and S293-Q307. In total, we observed 14 unique long-range interatomic contacts comprising 8 distinct residue pairs (*SI Appendix*, Table S3). Together, these long-range correlations indicate that the β1 strand packs against the β5 strand whereas β3 packs against β4. Consistent with these interstrand contacts, we also observed resolved Cγ chemical shifts for the 2 methyl groups of V306, V309, and V318, indicating that these Val side chains are located at steric zipper interfaces, unable to undergo χ_1 torsional motion. Therefore, the β-sheet core of 0N4R tau is shaped like a hairpin, with β1 and β5 marking the approximate beginning and end (Fig. 4*D*). At least one side of the hairpin is not straight, because the I278-V318 correlation and the G292-V309 correlation dictate that there are 14 residues in the R2 segment (from I278 to G292) but only 9 residues in the R3 segment (from V318 to V309) between these contacts. The additional 5 residues in R2 could be accommodated by a bulge in

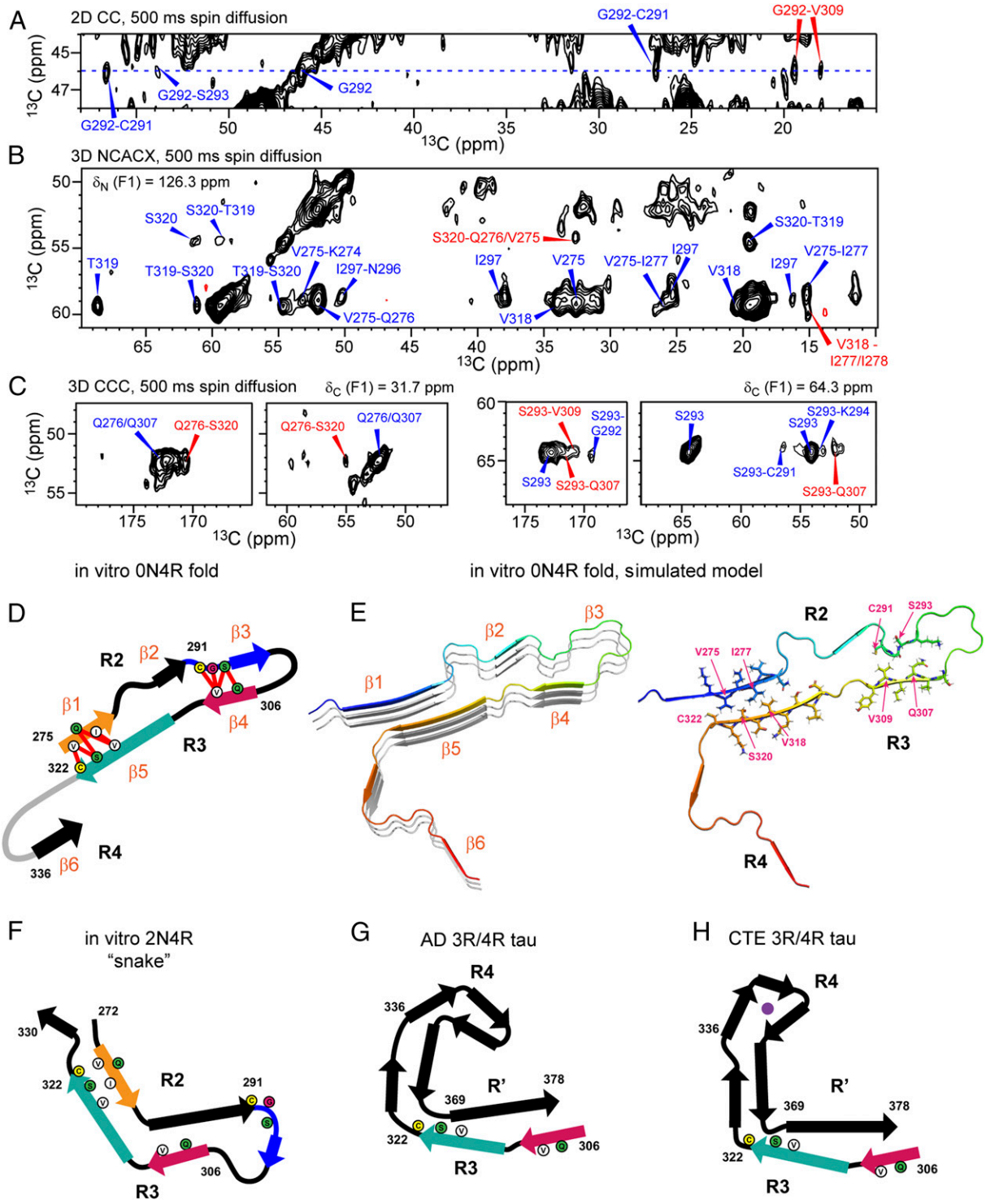

Fig. 4. Long-range cross-peaks from 2D and 3D NMR spectra for constraining the overall 3D fold of the β-sheet core of 0N4R tau fibrils. (*A*) Region of the 500-ms 2D ^{13}C-^{13}C spin diffusion spectrum, showing a G292-V309 cross-peak (assigned in red). (*B*) Region of the 3D NCACX spectra with 500-ms ^{13}C spin diffusion, showing cross-peaks between S320 and Q276/V275 and between V318 and I277/I278. (*C*) Representative F1 planes of the 3D CCC spectrum, measured with 500-ms spin diffusion between F2 and F3 dimensions. Q276-S320 cross-peaks and S293-Q307 cross-peaks are observed. (*D*) Schematic of the β-strands (thick arrows) and long-range correlations (red lines) measured in the SSNMR spectra. Gray lines indicate hypothetical locations of segments outside the R2–R3 core. Orange, blue, magenta, and green arrows highlight the crucial R2 hexapeptide motif, the C291-containing segment, the R3 hexapeptide motif, and the C322-containing segment. The same color scheme is used for the other schematics in *F*–*H*. (*E*) XPLOR-NIH lowest-energy structural fold of the 0N4R tau fibril core, calculated using dihedral angles and sparse long-range correlations. The β-strands were formed during simulated annealing and were not imposed. The backbone model on the left emphasizes the β-strand positions, and the model on the right shows the side-chain positions at the β1–β5 and β3–β4 steric zippers for which long-range correlations are observed. The exact side-chain positions are not fully determined by the data shown here, and thus this result should be taken as a low-resolution model. (*F*) Schematic of the cryo-EM 3D fold of the most common in vitro 2N4R polymorph called snake (14). The fibril core spans the R2–R3 domains, but C291 is located in a turn that is far from the R3 hexapeptide motif. (*G*) Schematic of the cryo-EM 3D fold of AD tau (10). The β-sheet core spans R3–R4 and part of the R′ domain. (*H*) Schematic of the 3D fold of the CTE 3R/4R mixed tau (15), which shares significant similarity with the AD structure.

R2 or by a bend of R2 and R3 toward R3. In either case R2 must traverse a longer distance than R3 between the long-range contacts, as schematically depicted in Fig. 4*D*.

To investigate the possible structures that are consistent with these experimental chemical shifts and long-range contacts, we conducted structure calculations for residues 268 to 340 in XPLOR-NIH (40), using chemical-shift restrained torsion angles and the sparse long-range contacts as input parameters. We assume parallel-in-register intermolecular packing, which is found in most amyloid fibrils to date (41). The lowest-energy structural model is shown in Fig. 4*E* while the next four low-energy structural models are illustrated in *SI Appendix*, Fig. S4. All five structural models show the experimentally observed β1–β5 and β3–β4 packing but vary in the length of the β-strands and the relative orientation of the two steric zippers. The lowest-energy model places the two steric zippers in an approximately parallel fashion and accommodates the length difference between the two sides of the hairpin shape by a bulge between β1 and β2 strands. In 4 of the 5 lowest-energy models, the C291 side chain lies at the steric zipper interface, close to the V309 side chain. In all 5 lowest-energy models, there is a bulge or turn at K280–L284 between the β1 and β2 strands and at K298–G304 between the β3 and β4 strands. These structural models are not identical to any of the 2N4R polymorphic structures (14). Although the 2N4R structures have the same β-strand stacking between the R2 hexapeptide motif and the center of R3, ^{318}VTS^{320}, none of the 2N4R folds packs the C291-containing segment with the R3 hexapeptide motif (Fig. 4*F*). Instead, the C291 segment is the most variable element in the 2N4R polymorphs. In comparison, the monomorphic 0N4R tau shows the C291 segment to be very rigid, manifesting some of the strongest intensities in the dipolar SSNMR spectra.

0N4R Tau Contains a Semirigid β-Sheet Domain outside the R2–R3 Fibril Core. While the solution-like ^{13}C TOCSY spectrum (Fig. 2*B*) and ^{1}H-^{15}N INEPT spectrum (Fig. 2*C*) indicate that some segments of fibrillar tau undergo large-amplitude near-isotropic motion, other correlation experiments depict a more complex dynamic landscape, with at least three other distinguishable domains (Fig. 5*A*). First, the Pro-rich P1 and P2 domains can be characterized as semimobile. Peaks with Pro-induced chemical shift changes have intensities that agree well with the amino acid distribution in the two termini and the Pro-rich domains. For example, there are 19 Ala's that do not precede a Pro residue and 2 Ala's that do in these domains (Fig. 5*B*). Consistently, the 2D TOCSY spectrum exhibits 2 resolved Ala Cα-Cβ cross-peaks with an intensity ratio of 10: 1. Similar X and X(P) chemical shift differences are observed for Ser, Thr, and Pro residues, whose intensity ratios also agree with the amino acid distribution in these terminal and Pro-rich domains (Fig. 5*C*). Therefore, the P1 and P2 domains are sufficiently mobile to give X(P) intensities in the TOCSY and INEPT spectra. At the same time, the dynamics of the P1 and P2 domains have restricted amplitudes, as shown by several dipolar correlation experiments. These experiments are designed to detect partly immobilized residues that are in close proximity to highly dynamic side chains. Pro signals feature prominently in these spectra. The basic experiment begins with selective excitation of side-chain ^{1}H signals at about 1.5 ppm and suppression of the rigid ^{1}H magnetization by a relaxation filter (*SI Appendix*, Fig. S5). The selected mobile-side-chain polarization is then transferred to the rigid residues by ^{1}H spin diffusion (16 ms) and ^{1}H-^{13}C CP. The resulting ^{13}C spectrum (Fig. 5*D*) shows a pronounced Pro Cδ peak at 48 ppm. The ^{13}C-^{1}H dipolar couplings of these mobile-side-chain transferred residues correspond to intermediate C–H order parameters (S_{CH}) of 0.2 to 0.6 (Fig. 5*E*). Moreover, when ^{13}C spin diffusion is allowed after the mobile-side-chain selection and polarization transfer, we found weak cross-peak intensities but strong diagonal intensities (Fig. 5*F*), indicating that ^{13}C spin diffusion is significantly attenuated by the mobility of the Pro-rich domains. Together, these data indicate that the P1 and P2 domains undergo fast anisotropic motions that are distinct from the near-isotropic mobility of the termini.

Compared with the Pro-rich domains, R1, R4, and R′ repeats are significantly more rigid but exhibit small-amplitude motions. This "semirigid" nature is manifested by the fact that residues in these domains show reasonably strong intensities in the ^{15}N-^{13}C correlation spectra at 260 K but attenuated intensities at higher temperatures (280–293 K) (Fig. 5*G* and *SI Appendix*, Fig. S6). S262 and T263 in R1 are two examples in this category, and 2 Ala residues also exhibit this temperature-dependent intensity change. The entire R1–R4 and R′ segment contains only 4 Ala residues, one Ala (A246) at the beginning of R1 and 3 Ala's in the middle of R′. Thus, the intensity reduction of 2 β-sheet Ala peaks at high temperature lends strong support to the semirigid nature of R1 and R′ repeats.

The β-sheet residues in R2 and R3 are fully immobilized, displaying strong signals in ^{15}N-^{13}C correlation spectra at both low and high temperatures (Fig. 5*G* and *SI Appendix*, Fig. S6). Measured ^{13}C-^{1}H dipolar couplings indicate S_{CH} order parameters close to 1.0 (*SI Appendix*, Fig. S7). The mobility difference between the R2–R3 segment and the R1 and R4–R′ segments is also supported by the peak intensities of the 3D NCACX spectrum; we can distinguish three categories of cross-peak intensities: strong, intermediate, and weak. While the β-strand residues generally exhibit stronger intensities than turns or disordered residues (Fig. 5*H*), many R1 and R4 residues display intermediate or weak intensities despite their β-sheet chemical shifts. Together, these data indicate that the rigid R2–R3 β-sheet core is surrounded by a semirigid matrix that includes part of R1, most of R4, and some of the R′ repeats.

We next measured the water accessibilities of the R2–R3 core and compared them with those of the semirigid R1 and R4–R′ domains using water-edited 2D ^{13}C correlation experiments (42). Interesting differences are observed in the water accessibilities of Ser and Cys residues (*SI Appendix*, Fig. S8*A*). For example, S258 and S341 are poorly hydrated whereas C291 and S352 are well hydrated. Ile peaks show low water-transferred intensities, indicating that the Ile side chains are buried in a hydrophobic core. The intensity ratios between the water-transferred spectrum and the full spectrum provide a semiquantitative measure of the different water accessibilities of the residues (*SI Appendix*, Fig. S8*B*). These hydration data are qualitatively consistent with the long-range correlations in indicating that the β-sheet core consists of R2–R3, largely surrounded by semirigid R1 and R4 repeats (*SI Appendix*, Fig. S8*C*).

Protease Contamination Can Induce Polymorphic Tau Fibrils. The protein samples used in this work are highly purified by HPLC (Fig. 6*A*), and this chemical homogeneity translates to structural homogeneity of the fibrillized samples. Indeed, ensuring very high purity of tau before and after fibrillization was critical for obtaining fibrils with a single morphology. On occasion, we obtained batches of tau fibrils with dramatically different ultrastructural morphologies from the structural model shown here by SSNMR. Fig. 6 illustrates one such sample. Negative-stain TEM images show twisted, straight, and curved filaments, with striking similarity to the polymorphic fibrils that were recently reported for 2N4R tau (Fig. 6*C*) (14). The heterogeneity in this aberrant sample was confirmed by trypsin digestion results, which show four bands ranging from 5 to 15 kDa in a Coomassie blue-stained SDS/PAGE gel (Fig. 6*B*). Low-molecular-weight fragments were observed even before trypsin digestion, indicating proteolysis during fibrillization (Fig. 6*B*). Upon addition of protease inhibitors to the fibrillization mixture (Fig. 6*B*), the monomorphic morphology of the straight filaments was restored (Fig. 6*C*),

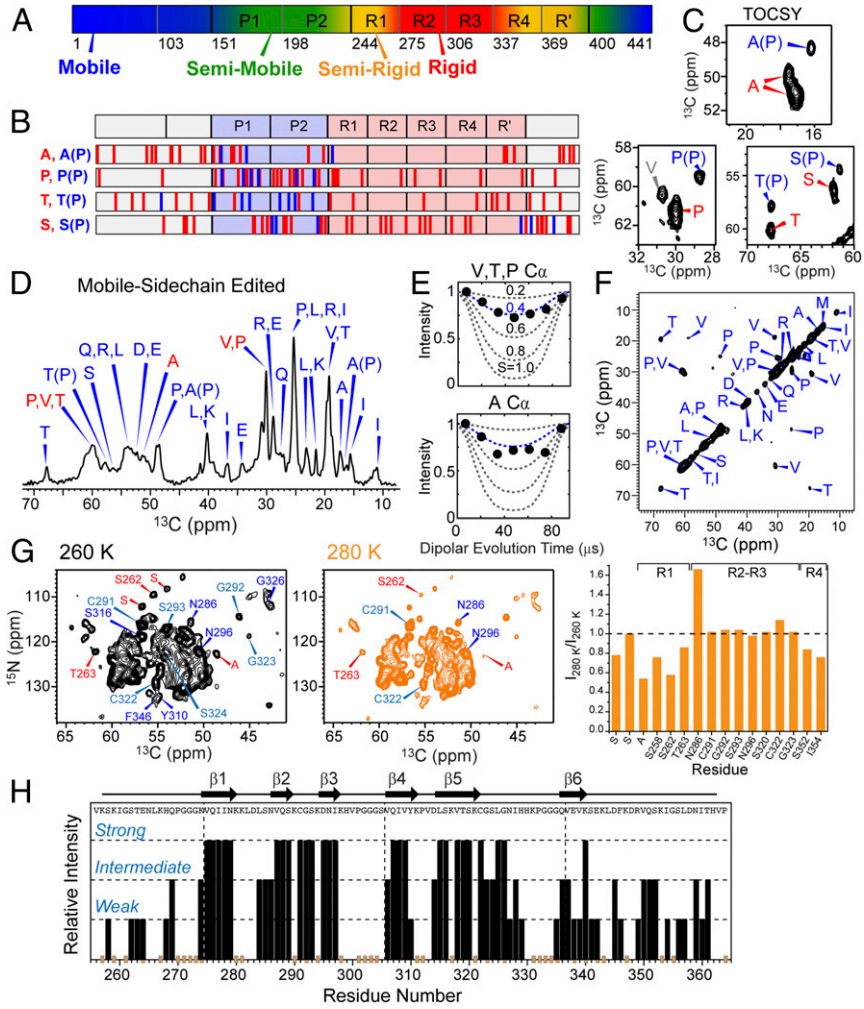

Fig. 5. The 0N4R tau fibrils exhibit heterogeneous dynamics. (*A*) Summary of the observed dynamic gradient in the protein. R2–R3 represents the rigid core. (*B*) Distribution of several residue types without and with a subsequent Pro. (*C*) Regions of the 2D ^{13}C-^{13}C TOCSY spectra, showing well-resolved signals of highly mobile residues without and with a subsequent Pro. (*D*) Mobile-side-chain transferred ^{13}C spectrum, showing prominent Pro peaks. (*E*) The ^{13}C-^{1}H DIPSHIFT curves of the mobile-side-chain transferred residues exhibit S_{CH} order parameters of about 0.4. (*F*) Mobile-side-chain transferred 2D ^{13}C spin diffusion spectrum with 64-ms mixing. A high-intensity diagonal is observed but few cross-peaks are present, indicating inefficient spin diffusion due to large-amplitude anisotropic motion of the Pro-rich domains. (*G*) Two-dimensional ^{15}N-$^{13}C\alpha$ correlation spectra measured at 260 K and 280 K. Residues in the R1 repeat (assigned in red) such as S262 and Ala show larger intensity reduction at high temperature compared with R2–R3 residues. The two Cys-containing triplets (cyan), ^{291}CGS^{293} and ^{322}CGS^{324}, display high intensities. The intensity ratios between the high- and low-temperature spectra are plotted on the right for a number of resolved signals. (*H*) Relative intensities of residues in the 3D NCACX spectrum. R2 and R3 residues have the highest intensities, whereas R1 and R4 residues have weaker average intensities, suggesting residual motion on the millisecond timescale.

together with a single trypsin-digestion band with a molecular weight matching the previously observed segment of residues 268 to 340 (Fig. 6*D*). Therefore, proteolytic fragmentation of tau induces polymorphic fibrils and should be carefully prevented in future work, because even small amounts of truncated or covalently modified protein can clearly lead to heterogeneity. In our hands, when proteolysis is prevented, heparin-fibrillized 0N4R has a predominant propensity to adopt a single structure at both the ultrastructural and the molecular level.

Discussion

The single set of β-sheet chemical shifts (*SI Appendix*, Fig. S9), together with a single dominant ultrastructural morphology (Figs. 1 and 6), provide strong evidence that heparin-fibrillized 4R tau adopts a single conformation in the fibril core. The rigid β-sheet core spans approximately residues 270 to 340 based on the assigned NMR chemical shifts, in good agreement with the trypsin digestion data. The conformational homogeneity contrasts the polymorphic structures reported recently for 2N4R tau (14). It is known that short tau peptides such as the R3 peptide alone self-assemble much faster than full-length tau and can template the aggregation of longer tau constructs (43). It is thus plausible that proteolytic fragments during fibrillization could alter the aggregation pathway of the protein, leading to polymorphic fibrils. In addition, the concentrations of heparin, salt, and tau monomers also affect fibril growth kinetics, and strong interactions between tau and heparin could promote the formation of multiple kinetically trapped structures (44). Further investigations of the fibril growth kinetics and the resulting structures will be valuable to gain insight into the folding landscape and pathological aggregation of tau in vivo.

The present SSNMR data on the straight filaments indicate that the rigid core of in vitro 0N4R tau fibrils spans R2 and R3 and adopts a single 3D fold that differs from the brain-derived tau fibrils (10, 11, 15) and from the 2N4R fibrils (14). The 0N4R fold shows the C291-containing β3 strand to be

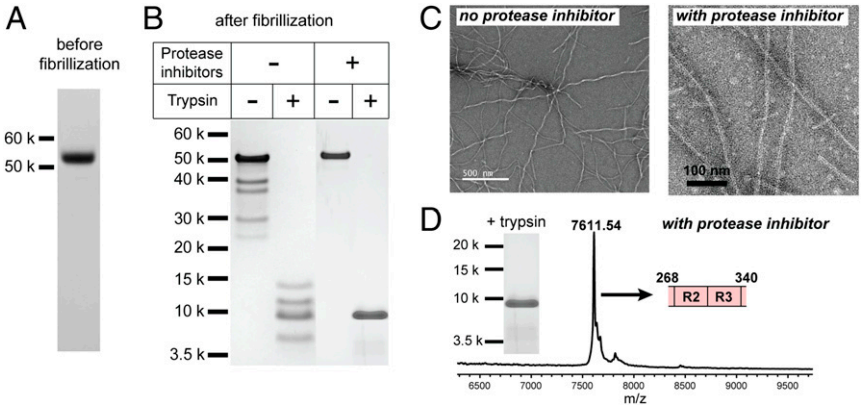

Fig. 6. Biochemical characterization of 0N4R tau fibrils formed with heparin in the absence or presence of protease inhibitors. (*A*) SDS/PAGE with Coomassie blue staining of purified 0N4R tau monomers. A single band is observed, indicating high purity. The protein appears larger than its molecular weight of 40 kDa due to the large number of basic residues. (*B*) SDS/PAGE gel of tau fibrils before and after trypsin digestion. In the absence of protease inhibitors, multiple proteolytic fragments were observed. The addition of protease inhibitors led to a single band both before and after trypsin digestion. (*C*) Negative-stain TEM images of heparin-fibrillized 0N4R tau. In the absence of protease inhibitors, multiple morphologies, including twisted, straight, and curved filaments, are observed. In the presence of protease inhibitors, only straight fibrils were observed. (*D*) Mass spectrum of trypsin-digested fibrils formed in the presence of protease inhibitors. A single peak corresponding to residues 268 to 340 is observed, consistent with the mass spectrum (Fig. 1*D*) for the samples used for SSNMR.

stacked against the β4 strand formed by the R3 hexapeptide motif ^{306}VQIVYK^{311}. None of the 2N4R tau polymorphs show this antiparallel steric zipper; instead, they show the C291–I297 segment to be conformationally variable and not interacting with the R3 hexapeptide motif. This suggests that the C291-containing segment is structurally plastic in response to environmental changes. In comparison, both the 0N4R fold and the 2N4R structures share a common steric zipper between the R2 hexapeptide motif and the C322-containing β5 strand in the middle of R3. The fact that this β1–β5 stacking is observed in both constructs suggests that this interaction is extremely stable and may be a good target for anti-tau inhibitors (45).

The monomorphic nature of the in vitro 4R tau observed here differs from several recent biophysical studies of 4R tau (46, 47). The discrepancy may result from the different protein constructs used as well as differences in the fibril-forming conditions. For example, double electron–electron resonance (DEER) distance measurements of a truncated 4R tau (residues 255 to 441) showed broad distributions (3.0 to 4.9 nm) of distances between MTSL (2,2,5,5-tetramethyl-1-oxyl-3-methyl methanethiosulfonate) electron spin labels tethered to cysteine residues that were incorporated into the protein by site-directed mutagenesis (46). Most spin-labeled pairs were placed into R3 and R4 repeats, which straddle the rigid and semirigid domains of the protein as revealed here. Thus, the large distance distribution may in part reflect true disorder of the R4 repeat. However, since these spin-labeling experiments require the mutation of the two native C291 and C322, which occur in the two most rigid β-strands of the protein, the mutation may affect the structural homogeneity of 4R tau. The wild-type sequence also shows a broad distance distribution between C291 and C322, suggesting that truncation of the N-terminal half of the protein and/or the fibrillization condition may reduce the structural homogeneity of the fibril core. Another DEER electron paramagnetic resonance study of full-length 2N4R tau fibrils obtained by seeded growth found a broad distance distribution between K311 and I328 (47). Although K311 is exposed to the surface of the β-sheet core in the AD tau structure, within in vitro 4R tau it is located in a spatially constricted region between the β4 and β5 strands. Therefore, we hypothesize that incorporation of the MTSL label at this site might affect the fibril structural homogeneity.

What is the potential significance of the present in vitro 4R tau fold for the structures of brain-derived tau fibrils? Fig. 4 *G* and *H* depicts the 3D folds of 3R/4R mixed tau structures found in AD and CTE in comparison with the 0N4R tau fold and the most common in vitro 2N4R tau fold. All 3D folds of these tau samples can be qualitatively described as a C- or hairpin-shape; however, the β-sheet cores span very different segments of the four microtubule-binding repeats. In 3R/4R mixed tau, the C-shape encompasses the R3 and R4 repeats and a small segment of R′. In the pure 4R tau, the fibril core spans R2 and R3 repeats. The 3R tau from PiD has the most expanded fibril core, spanning R1, R3, R4, and a small portion of R′ (11). Therefore, R3 is universally conserved among all in vivo and in vitro tau fibril cores known so far. To gain insight into whether the in vitro 4R tau structural fold determined here is potentially relevant to in vivo 4R tau structures, we compare the known 3D structures of tau fibrils with trypsin digestion data (23). In the 3R/4R AD tau, the shortest trypsin-resistant fragment of tau ranges from residue H299 to K385, in good agreement with the cryo-EM structures, which span residues 306 to 378 (10) (Fig. 4*G*). For the 3R tau of PiD, the trypsin-resistant tau fragment spans residues L243 to K385, also in good agreement with the cryo-EM structure that spans residues 254 to 378 (11). These comparisons suggest that trypsin digestion data accurately report the β-sheet core of diseased tau fibrils, so that we can use available trypsin digestion data of 4R tauopathies to infer the relevance of the in vitro 0N4R structural fold. In the 4R tau diseases of PSP and corticobasal degeneration, the shortest trypsin-resistant fragment was reported to span residues H268 to K369, or R2–R4 domains. The 0N4R tau fibrils studied here have a shorter trypsin-resistant core that spans residues 268 to 340 (R2 and R3) (Fig. 1*D*). However, we detected β-sheet signals from the R4 repeat, although their intensities are weaker than the R2–R3 β-sheet signals (Fig. 5*H*). Therefore, in vitro and in vivo 4R tau fibrils most likely share the same rigid R2–R3 core, but the in vivo 4R tau fibrils may contain a more rigid R4 segment than the in vitro 4R tau fibril studied here.

A potential reason for the variations in the exact length and fold of the rigid β-sheet core among tau fibrils is the electrostatic interactions between the highly charged dynamic domains of the protein and the β-sheet core. The current SSNMR data indicate a complex dynamical landscape in which the two Pro-rich segments undergo anisotropic motions with intermediate order parameters of 0.2 to 0.6, making ^{13}C spin diffusion inefficient, whereas the R1, R4, and R′ repeats undergo small-amplitude

motion on the millisecond timescale, which cause temperature-dependent intensities in the ^{15}N-^{13}C correlation spectra (Fig. 5 *G* and *H*). The protein thus exhibits a dynamical gradient with respect to the amino acid sequence, becoming increasingly mobile from the R2–R3 core toward the two termini. Importantly, chemical shift data indicate that the semirigid R1 and R4 repeats retain β-sheet character, implying that these repeats may interact with the well-ordered R2–R3 β-sheet core even though they do not form long hydrogen-bonded chains along the fibril axis. This semirigid R1 and R4 domain is partly shielded from trypsin digestion (23). Its difference from the more mobile termini is also suggested by the disordered electron densities in cryo-EM maps of AD, PiD, and 2N4R fibrils (10, 11, 14) and by the absence of solution NMR signals for residues in these domains in 2N4R tau protofibrils (25). The current SSNMR data provide a first definition of the conformational dynamics of this domain.

In conclusion, the current SSNMR study provides a view of the overall 3D fold, the structural homogeneity, and the dynamics of fibrils formed by a full-length 4R tau. Our data show that intact heparin-fibrillized 0N4R tau adopts a single β-sheet conformation for the fibril core. This fibril core possesses a steric zipper between the R2 hexapeptide motif and the middle of the R3 repeat, near residue C322. The fibril core also contains a second steric zipper between the C291-containing segment in R2 and the R3 hexapeptide motif. This second steric zipper structure is sensitive to environmental changes during fibril growth, as shown by the polymorphic 2N4R structures. The rigid R2–R3 β-sheet core is surrounded by β-sheet–rich R1 and R4 repeats, which undergo small-amplitude motions on the millisecond timescale, whereas the Pro-rich domains exhibit large-amplitude anisotropic motions, culminating in nearly isotropically mobile termini. Future studies will focus on higher-resolution structure determination of the fibril core.

Materials and Methods

Uniformly ^{13}C, ^{15}N-labeled 0N4R tau with reverse G, E, K labeling was expressed in *Escherichia coli* and purified using cation exchange chromatography and reversed-phase HPLC. Fibrils were formed by shaking 0.4 mg/mL tau monomer solution containing 0.125 mg/mL heparin at 37 °C for 3 d. Negative-stain EM and trypsin fingerprinting were used to characterize the fibril morphology and the rigid core. SSNMR spectra were measured primarily on 800-MHz spectrometers both at the National High Magnetic Field Laboratory (NHMFL) and at the Francis Bitter Magnet Laboratory (FBML) (*SI Appendix*, Table S4). A small number of spectra were also measured on 600-MHz and 900-MHz spectrometers in the FBML. Three-dimensional NCACX, NCOCX, and CONCA correlation spectra were used for resonance assignment of the fibril core. Long-mixing-time 2D CC, 3D CCC, and 3D NCACX spectra were measured to obtain long-range correlations. Secondary chemical shifts were calculated using TALOS-N (36). Simulated annealing was performed in XPLOR-NIH (40). Additional details are given in *SI Appendix*, *SI Methods*.

ACKNOWLEDGMENTS. This work is supported by NIH Grants AG059661 (to M.H.) and AG002132 (to W.F.D.). H.W. is supported by a CTSI TL1 Postdoctoral Fellowship (TL1TR001871). The NHMFL is supported by National Science Foundation Cooperative Agreement DMR-1644779 and the state of Florida. We thank Dr. Zhehong Gan for help with coordinating the experiments at the NHMFL. This study made use of NMRbox: National Center for Biomolecular NMR Data Processing and Analysis, a Biomedical Technology Research Resource, which is supported by NIH Grant P41GM111135 (National Institute of General Medical Sciences). We thank Julia Becker for help with cloning, Dr. Jan Stöhr for initial studies, and Prof. Sjors Scheres for sharing the coordinates of the 2N4R filaments.

1. E. H. Kellogg *et al.*, Near-atomic model of microtubule-tau interactions. *Science* **360**, 1242–1246 (2018).
2. C. M. Wischik *et al.*, Structural characterization of the core of the paired helical filament of Alzheimer disease. *Proc. Natl. Acad. Sci. U.S.A.* **85**, 4884–4888 (1988).
3. Y. Wang, E. Mandelkow, Tau in physiology and pathology. *Nat. Rev. Neurosci.* **17**, 5–21 (2016).
4. M. Goedert, D. S. Eisenberg, R. A. Crowther, Propagation of tau aggregates and neurodegeneration. *Annu. Rev. Neurosci.* **40**, 189–210 (2017).
5. O. A. Morozova, Z. M. March, A. S. Robinson, D. W. Colby, Conformational features of tau fibrils from Alzheimer's disease brain are faithfully propagated by unmodified recombinant protein. *Biochemistry* **52**, 6960–6967 (2013).
6. M. Goedert, M. Masuda-Suzukake, B. Falcon, Like prions: The propagation of aggregated tau and α-synuclein in neurodegeneration. *Brain* **140**, 266–278 (2017).
7. B. Falcon *et al.*, Conformation determines the seeding potencies of native and recombinant Tau aggregates. *J. Biol. Chem.* **290**, 1049–1065 (2015).
8. A. T. Petkova *et al.*, Self-propagating, molecular-level polymorphism in Alzheimer's beta-amyloid fibrils. *Science* **307**, 262–265 (2005).
9. R. Tycko, Amyloid polymorphism: Structural basis and neurobiological relevance. *Neuron* **86**, 632–645 (2015).
10. A. W. P. Fitzpatrick *et al.*, Cryo-EM structures of tau filaments from Alzheimer's disease. *Nature* **547**, 185–190 (2017).
11. B. Falcon *et al.*, Structures of filaments from Pick's disease reveal a novel tau protein fold. *Nature* **561**, 137–140 (2018).
12. B. Falcon *et al.*, Tau filaments from multiple cases of sporadic and inherited Alzheimer's disease adopt a common fold. *Acta Neuropathol.* **136**, 699–708 (2018).
13. M. Goedert *et al.*, Assembly of microtubule-associated protein tau into Alzheimer-like filaments induced by sulphated glycosaminoglycans. *Nature* **383**, 550–553 (1996).
14. W. Zhang *et al.*, Heparin-induced tau filaments are polymorphic and differ from those in Alzheimer's and Pick's diseases. *eLife* **8**, e43584 (2019).
15. B. Falcon *et al.*, Novel tau filament fold in chronic traumatic encephalopathy encloses hydrophobic molecules. *Nature* **568**, 420–423 (2019).
16. J. X. Lu *et al.*, Molecular structure of β-amyloid fibrils in Alzheimer's disease brain tissue. *Cell* **154**, 1257–1268 (2013).
17. W. Qiang, W. M. Yau, J. X. Lu, J. Collinge, R. Tycko, Structural variation in amyloid-β fibrils from Alzheimer's disease clinical subtypes. *Nature* **541**, 217–221 (2017).
18. J. Rasmussen *et al.*, Amyloid polymorphisms constitute distinct clouds of conformational variants in different etiological subtypes of Alzheimer's disease. *Proc. Natl. Acad. Sci. U.S.A.* **114**, 13018–13023 (2017).
19. C. Condello *et al.*, Structural heterogeneity and intersubject variability of Aβ in familial and sporadic Alzheimer's disease. *Proc. Natl. Acad. Sci. U.S.A.* **115**, E782–E791 (2018).
20. A. T. Petkova, W. M. Yau, R. Tycko, Experimental constraints on quaternary structure in Alzheimer's beta-amyloid fibrils. *Biochemistry* **45**, 498–512 (2006).
21. A. K. Paravastu, R. D. Leapman, W. M. Yau, R. Tycko, Molecular structural basis for polymorphism in Alzheimer's beta-amyloid fibrils. *Proc. Natl. Acad. Sci. U.S.A.* **105**, 18349–18354 (2008).
22. M. R. Elkins *et al.*, Structural polymorphism of Alzheimer's β-amyloid fibrils as controlled by an E22 switch: A solid-state NMR study. *J. Am. Chem. Soc.* **138**, 9840–9852 (2016).
23. S. Taniguchi-Watanabe *et al.*, Biochemical classification of tauopathies by immunoblot, protein sequence and mass spectrometric analyses of sarkosyl-insoluble and trypsin-resistant tau. *Acta Neuropathol.* **131**, 267–280 (2016).
24. S. Wegmann, I. D. Medalsy, E. Mandelkow, D. J. Müller, The fuzzy coat of pathological human Tau fibrils is a two-layered polyelectrolyte brush. *Proc. Natl. Acad. Sci. U.S.A.* **110**, E313–E321 (2013).
25. S. Bibow *et al.*, The dynamic structure of filamentous tau. *Angew. Chem. Int. Ed. Engl.* **50**, 11520–11524 (2011).
26. M. D. Mukrasch *et al.*, Structural polymorphism of 441-residue tau at single residue resolution. *PLoS Biol.* **7**, e34 (2009).
27. M. Schwalbe *et al.*, Predictive atomic resolution descriptions of intrinsically disordered hTau40 and α-synuclein in solution from NMR and small angle scattering. *Structure* **22**, 238–249 (2014).
28. S. Barghorn, J. Biernat, E. Mandelkow, Purification of recombinant tau protein and preparation of Alzheimer-paired helical filaments in vitro. *Methods Mol. Biol.* **299**, 35–51 (2005).
29. D. S. Wishart, C. G. Bigam, A. Holm, R. S. Hodges, B. D. Sykes, 1H, 13C and 15N random coil NMR chemical shifts of the common amino acids. I. Investigations of nearest-neighbor effects. *J. Biomol. NMR* **5**, 67–81 (1995).
30. M. Sanz-Hernández, A. De Simone, The PROSECCO server for chemical shift predictions in ordered and disordered proteins. *J. Biomol. NMR* **69**, 147–156 (2017).
31. M. Baldus, A. T. Petkova, J. Herzfeld, R. G. Griffin, Cross polarization in the tilted frame: Assignment and spectral simplification in heteronuclear spin systems. *Mol. Phys.* **95**, 1197–1207 (1998).
32. M. Hong, Resonance assignment of 13C/15N labeled solid proteins by two- and three-dimensional magic-angle-spinning NMR. *J. Biomol. NMR* **15**, 1–14 (1999).
33. C. M. Rienstra, M. Hohwy, M. Hong, R. G. Griffin, 2D and 3D 15N-13C-13C NMR chemical shift correlation spectroscopy of solids: Assignment of MAS spectra of peptides. *J. Am. Chem. Soc.* **122**, 10979–10990 (2000).
34. I. Hung, Z. Gan, Spin-locking and cross-polarization under magic-angle spinning of uniformly labeled solids. *J. Magn. Reson.* **256**, 23–29 (2015).
35. M. von Bergen, S. Barghorn, J. Biernat, E. M. Mandelkow, E. Mandelkow, Tau aggregation is driven by a transition from random coil to beta sheet structure. *Biochim. Biophys. Acta* **1739**, 158–166 (2005).
36. Y. Shen, A. Bax, Protein backbone and sidechain torsion angles predicted from NMR chemical shifts using artificial neural networks. *J. Biomol. NMR* **56**, 227–241 (2013).
37. O. C. Andronesi *et al.*, Characterization of Alzheimer's-like paired helical filaments from the core domain of tau protein using solid-state NMR spectroscopy. *J. Am. Chem. Soc.* **130**, 5922–5928 (2008).

38. V. Daebel *et al*., β-Sheet core of tau paired helical filaments revealed by solid-state NMR. *J. Am. Chem. Soc.* **134**, 13982–13989 (2012).
39. S. Xiang *et al*., A two-component adhesive: Tau fibrils arise from a combination of a well-defined motif and conformationally flexible interactions. *J. Am. Chem. Soc.* **139**, 2639–2646 (2017).
40. C. D. Schwieters, J. J. Kuszewski, N. Tjandra, G. M. Clore, The Xplor-NIH NMR molecular structure determination package. *J. Magn. Reson.* **160**, 65–73 (2003).
41. M. D. Gelenter *et al*., The peptide hormone glucagon forms amyloid fibrils with two coexisting β-strand conformations. *Nat. Struct. Mol. Biol.* **26**, 592–598 (2019).
42. T. Wang, H. Jo, W. F. DeGrado, M. Hong, Water distribution, dynamics, and interactions with Alzheimer's β-amyloid fibrils investigated by solid-state NMR. *J. Am. Chem. Soc.* **139**, 6242–6252 (2017).
43. J. Stöhr *et al*., A 31-residue peptide induces aggregation of tau's microtubule-binding region in cells. *Nat. Chem.* **9**, 874–881 (2017).
44. H. L. Zhu *et al*., Quantitative characterization of heparin binding to tau protein: Implication for inducer-mediated tau filament formation. *J. Biol. Chem.* **285**, 3592–3599 (2010).
45. P. M. Seidler *et al*., Structure-based inhibitors of tau aggregation. *Nat. Chem.* **10**, 170–176 (2018).
46. Y. Fichou, M. Vigers, A. K. Goring, N. A. Eschmann, S. Han, Heparin-induced tau filaments are structurally heterogeneous and differ from Alzheimer's disease filaments. *Chem. Commun. (Camb.)* **54**, 4573–4576 (2018).
47. H. A. Weismiller *et al*., Structural disorder in four-repeat tau fibrils reveals a new mechanism for barriers to cross-seeding of tau isoforms. *J. Biol. Chem.* **293**, 17336–17348 (2018).